Electric field enhancement in ceramic capacitors due to interface amplitude roughness.

James P. Heath, John H. Harding, Derek C. Sinclair and Julian S. Dean[*]

Department of Materials Science & Engineering, University of Sheffield, Sir Robert Hadfield Building, Mappin Street, Sheffield S1 3JD, UK

Abstract:

The electrical behaviour of the interface between the ceramic and electrode layers in multi layer ceramic capacitors has been studied using finite element modelling. Interface models were produced with varying amplitudes of roughness based upon analysis of micrographs both captured in-house and from the literature. The impedance responses, direct current electric field and current density distributions of the different interfaces were compared. Increasing the root-mean-squared amplitude roughness from 0 to 0.16 μm increased the maximum field strength by over a factor of four. The electric field distribution showed that fluctuations in the increase of field strength were due to local interface morphology. Sharp intrusions of the electrode into the ceramic layer resulted in particularly large field enhancements and should be avoided to reduce the likelihood of device breakdown.

1. Introduction:

Market demands have put significant constraints on electrical components. There is a drive to miniaturise components without compromising performance or reliability. One example of this is the multi layer ceramic capacitor (MLCC). To maintain the reliability of MLCCs, rare earth elements (REE) have been added as dopants to barium titanate ceramics used in the dielectric layers. This doping increases the reliability of the device[1] and also the temperature stability of capacitance[2]. The price of the REEs is susceptible to market fluctuations and there has been increasing concern about the environmental impact of their extraction[3]. It would be preferable to improve the reliability of devices such as MLCCs without having to resort to expensive and polluting REEs or at least limit their use. For this purpose, we report on some microstructural contributions to device reliability.

The MLCC is a lamellar device composed of alternating layers of ceramic dielectric and base metal electrode (see fig. 1A) to give a high capacitance to volume ratio. Due to the large volume of MLCCs required every year (billions of units[1]) the devices must be made rapidly and at low cost. This results in a rough interface between the ceramic and electrode layers (see fig. 1B). Here, the effect of interface roughness on the electrical properties and reliability of MLCCs will be explored using finite element modelling (FEM).

A FEM code developed to simulate the electrical response of a 3D microstructure has been reported previously[4, 5]. We employ this code to analyse

---

[*] Corresponding author.
Email: j.dean@sheffield.ac.uk

the response of the interface between a ceramic and electrode layer within a MLCC. The model is simplified to consist of a two-micron cube, centred at the metal/ceramic interface (see fig. 1C). An idealised flat interface is compared to interfaces of increasing roughness. To facilitate discussion, the flat section of the ceramic layer will be referred to as the top of the microstructure and the flat region of the electrode as the bottom.

In this study the amplitude of interface roughness will be the primary concern as a previous study of this microstructural feature was limited to analytical calculations and FEM simulations of idealised sinusoidal electrodes[6]. Samantaray *et al.* have performed extensive FEM studies using serial sectioning of real MLCCs[7], which focuses on electrode discontinuity. To the best of our knowledge, studies on the amplitude of interface roughness have not been undertaken for more realistic randomised interfaces.

A.   B.   C.
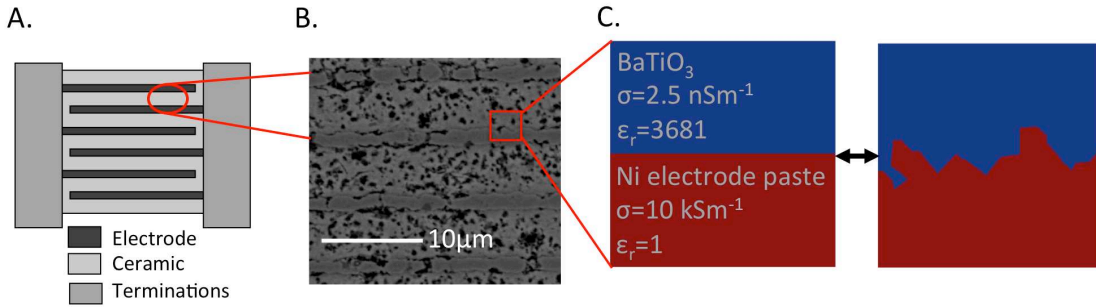
Fig. 1. (A) Schematic of a multi layer ceramic capacitor. (B) Micrograph of capacitor microstructure at electrode/ceramic interface obtained from a proto-type device in-house. (C) Cross section of the geometry of flat and rough interface models.

2. Modelling methodology:

The electrical characterisation of the interfaces was simulated using the finite element method (FEM). The in-house code used in this study, solves for the electric potential (φ) in the time domain using the Galerkin scheme for time discretisation. By assuming each material simulated is linear, isotropic and has no time dispersion, the potential can be solved as function of space ($\boldsymbol{r}$) and time (t) for given values of conductivity (σ) and permittivity (ε) assigned to the elements of the mesh. This allows conductive and Debye relaxations to be simulated. To replicate electrical measurements a potential difference is applied to model using a Dirichlet boundary condition (known values of potential at the top and bottom of the model). The local current density ($\boldsymbol{j}$) is solved as function of potential using equation (1):

$$\nabla.\boldsymbol{j} = -\nabla.\left(\sigma\nabla\varphi(\boldsymbol{r}, t) + \varepsilon(\boldsymbol{r})\frac{\delta}{\delta t}\nabla\varphi(\boldsymbol{r}, t) \right) (1)$$

A thorough derivation of the above equation and the assumptions in the model can be found in our methods paper[4]. A surface integral of the local current density at the top of the model is then used to find the current flowing into the model.

In addition to the Dirichlet condition a Neumann boundary condition was applied to the free sides of the model setting current density to zero thus confining the current to the simulated microstructure. Ideally the Dirichlet condition would be applied across at whole ceramic layer with two electrode/ceramic interfaces, however given the large amount of elements required to mesh a single interface (see supplementary information) the simulation of multiple interfaces is computationally impractical. The conditions in this study are a reasonable approximation when assuming the ceramic layers are thicker than the electrode layer (as the potential will become more homogenous in the centre of the ceramic layer) and the simulated area is located close to the centre of the capacitor away from the electrode margins (as it has been shown the potential is very heterogeneous near the margins). The conditions used here are relevant to other ceramic/metal interfaces that are perpendicular to an applied potential difference.

The mesh size used in this work was defined by a convergence study, which is detailed in the supplementary information. Mesh size at the interface was set to 7.5 nm, growing exponentially with distance further from the interface using an exponent of 2.25. This generates mesh divisions at the extremities of the model of 0.13 μm. This resulted in models consisting of ~4.5 million elements. The meshing was achieved using Gmsh[8]. The value for the maximum local field strength for a given interface was defined as the border of the top 99.95th percentile of electric field strength. Higher percentiles were found to be susceptible to numerical error and as such are not reported here. The 99.95th percentile provides suitable lower bound for the maximum intensification of the electric field by microstructural features while low enough to ensure convergence of the value.

To replicate the highly accelerated lifetime tests used to study the reliability of capacitors, the DC electric field distribution was calculated for a static applied voltage of 142V. Local values of electric field were acquired instantaneously after the DC simulation had reached steady state. AC impedance spectra were simulated in the frequency range from 0.05 Hz to 10 MHz with an applied sinusoidal voltage of 100 mV. The material properties for the ceramic[9] and the electrode[10] were taken from the literature and were assigned to individual elements depending on the elements' location. The ceramic was assigned a conductivity of 2.5 nSm^{-1} and a relative permittivity of 3681. The electrode was assigned a conductivity of 10 kSm^{-1} and a relative permittivity of 1.

To generate a rough interface in our models, we produce a 2μm long cube consisting of ~1200 Voronoi tessellated regions[11] (see fig. 2A). A definable plane is then set through the centre of the cube. If the centroid of each region is, for example, above this centre plane, it would be assigned the properties of the ceramic, if below, then of the electrode material. This method of using defined Voronoi regions allows the roughness to take on a realistic granular structure. To generate different levels of roughness amplitude we modify how the regions are assigned their properties. To achieve this the plane is divided into a grid, (as shown in fig. 2A) of 8x8 sectors. Each sector has a random number attributed to it that ranges from zero to the maximum allowed amplitude. Any region whose centroid is within the sector and above the random value is then given ceramic properties, and any below given electrode properties. This is then repeated for each sector allowing a greater degree of roughness to be introduced. By varying

the value of the maximum amplitude, different values of roughness can be created. Due to the large number of Voronoi regions it was possible to produce a range of values of roughness that did not interact with the boundary of the simulation.

        To characterise the roughness of such a system, the maximum amplitude is insufficient as the value only describes one point, which may not be representative of the whole interface. One method to characterise the amplitude of a rough surface is the root-mean-squared amplitude (S_q). This is commonly used in surface science[12]. Here we apply this approach to interfaces by considering the ceramic/electrode interface as an open surface and measuring its amplitude as the point where a hard sphere, projected vertically towards the electrode material, first touches the surface. In surface science, S_q would be measured using profilometry experiments such as atomic force microscopy (AFM). Using the hard sphere mimics the finite radius of an AFM tip. Here a sphere of 50 nm diameter was used, comparable to experimental tips[13]. To calculate S_q, first the residual interface must found at N by M measured points:

$$\eta^2(x_i, y_j) = \left(\bar{Z} - Z(x_i, y_j)\right)^2 \quad (2)$$

where Z is the interface amplitude at coordinates (x_i, y_j) and $\bar{Z}$ is the mean interface amplitude (see fig. 2B) and therefore the nominal position of the equivalent flat interface. S_q is the standard deviation of all measured surface residuals:

$$S_q = \sqrt{\frac{1}{MN} \sum_{j=1}^{N} \sum_{i=1}^{M} \eta^2(x_i, y_j)} \quad (3)$$

To measure the amplitude across the entire interface, we define the interface using a 200 by 200 grid of points (see fig. 2A) and S_q is calculated by measuring the interface amplitude at each point using a simulated sphere as described above. This density of grid points gave a lateral resolution of 10 nm, which is achievable with experimental AFM[14]. Hence the mean interface amplitude can be calculated as can the residual interface amplitude at each point. This gave S_q values ranging from 0.08 to 0.16 µm for a defined maximum grain centroid amplitude of 0.05 to 0.15 µm, respectively.
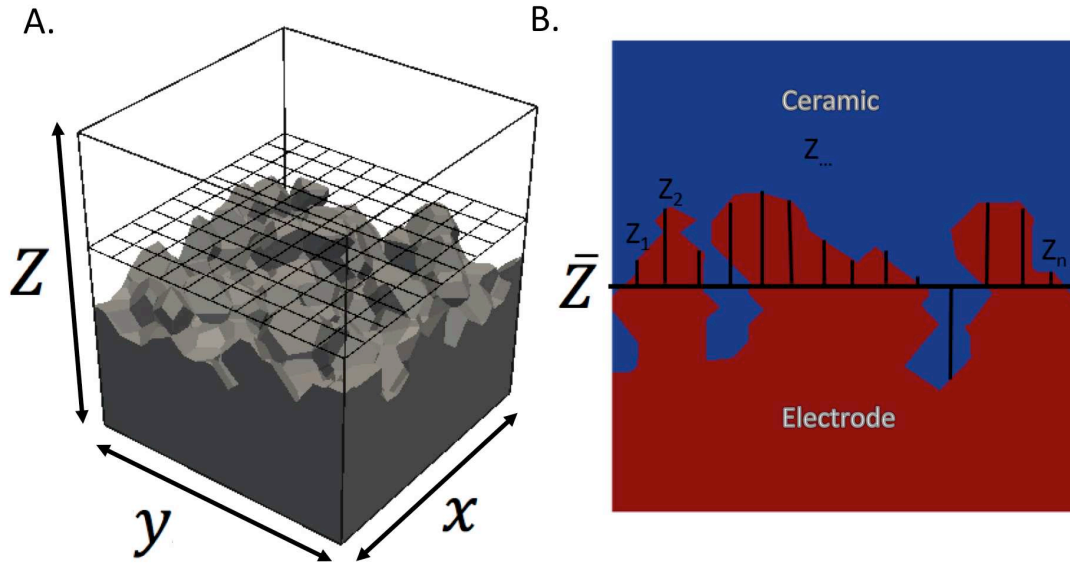
Fig. 2. (A) Meshed model of a rough interface with ceramic layer removed for visualisation with a grid showing how the amplitude is assigned and how the interface is divided for RMS analysis (note the grid used for analysis was finer). (B) Schematic of interface showing how the amplitudes of the interface are measured from a plane normal to the Z axis that bisects the model.

Ideally these S_q values would be directly compared with those for real devices. However, this requires tomography data using highly specialised equipment that is time-consuming and expensive[15]. A more pragmatic approach is the analysis of 2D micrographs of ceramic/electrode multilayers using Matlab's image processing toolbox[16]. Micrographs were converted into a binary image and the Prewitt algorithm[17] was used to find the outline of the interface (see fig. 3). Smaller features such as pores were removed using Matlab's *bwareaopen* function. If any of the previous steps caused visible changes to the interface region the micrograph was excluded from the analysis. 21 interfaces were successfully analysed from micrographs taken from the literature[18, 19, 20, 21, 22]. These covered a wide range of capacitors: from industry standard barium titanate (BT) MLCCs to laboratory-produced multilayers using experimental compositions. An additional six interfaces were obtained from industrial samples measured in-house. Cross sections of the MLCCs were observed using scanning electron microscopy (TM3030 Plus SEM, Hitachi, Hitachi High-Technologies Europe GmbH, Krefeld, Germany). Once a satisfactory interface had been obtained, a 2D equivalent of the hard sphere probe (hence a hard circle here) was used to measure the interface amplitude of the electrode. The circle diameter was set to 50 nm and the interface amplitudes measured 100 times per micron in 10 nm increments to maintain equivalence with the 3D version. R_q, the 2D equivalent of S_q, could then be calculated using equation 4.

$$R_q = \sqrt{\frac{1}{N} \sum_{i=1}^{N} \eta^2(x_i)} \quad (4)$$

The equivalence of equations 3 and 4 can be appreciated since S_q is effectively a combination of R_q line scans into and out of the plane of a given micrograph. Providing the roughness is isotropic in nature these values are comparable[23].

Fig. 3 shows this process for several interfaces on the same MLCC. The interfaces in this microstructure that were analysed are given in fig. 3A and marked i - x. A green box indicates an area that was successfully analysed and the number next to it is the measured R_q value in microns. Red boxes indicate that Matlab's image processing algorithms could not detect the interface; an example of a failed binary image is given in fig. 3B. Orange boxes indicate an area that was neglected for analysis, as there was low continuity between the electrode and ceramic. Interfaces with high and low R_q values are shown in figs. 3C and D, respectively. From top to bottom the three parts consist of: the interface in the original micrograph considered, the extracted interface and finally the extracted interfaces together with the hard circle profile.

For this analysis the micrographs were aligned so the electrode layers were horizontal. However, there was also sinusoidal variation in the interface amplitude occurring over a larger length scale than considered in the simulations of this work. To ensure the R_q values were comparable between the micrographs and simulated microstructures, the micrograph interfaces were rotated so the end points of the interface were level. The resulting rotated interfaces are shown as green lines on fig. 3C and D. If this rotation is not performed, smoother interfaces that are sloping have artificially high R_q values. For example, the interface in fig. 3C has little overall slope so applying the rotation operation only changes the R_q value from 0.142 to 0.146 μm. For fig. 3D, where the interface has a higher slope, the rotation decreases the R_q value from 0.151 to 0.070 μm.
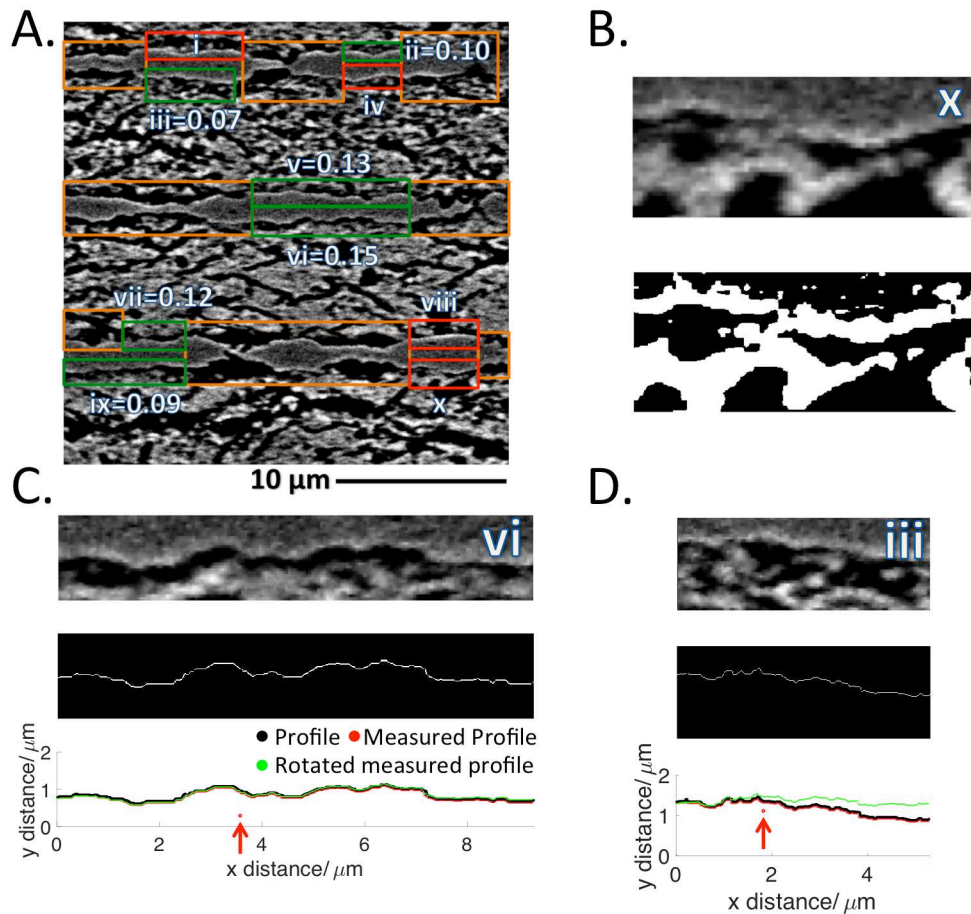
Fig. 3. Cross section of a BaTiO$_3$-based (BT) MLCC. (A) The original micrograph, with interfaces labelled i - x, highlighted with: *green* - interface successfully analysed with R_q value in microns; *orange* - region not included in analysis due to low interface continuity and *red* - interface not detectable by Matlab's image processing algorithms. (B) Example of an interface that could not be recognised, (top) original micrograph, (bottom) resultant binary image from Matlab. (C) Analysis of interface with R_q of 0.151 μm. From top to bottom: micrograph of area analysed, interface detected by Matlab algorithm and profile measured by hard circle. (D) Analysis of interface with R_q of 0.070 μm in the same format as (C). Note: the top right of (B-D) indicates the position on (A) and for (C and D) an arrow indicates the direction of the hard circle's movement towards the interface with the circle drawn to scale.

A summary of all R_q values obtained is presented in fig. 4A. R_q values for industrial BT MLCCs[18, 19] are between 0.037 to 0.097 μm. For industrial BT MLCCs made with experimental ceramic compositions that had poor adhesion between the electrode and ceramic as presented in fig. 3, R_q could be up to 0.151 μm. Laboratory-produced BT[20, 22] and non-BT MLCCs[21] varied significantly, with R_q values up to 0.700 μm. As the ceramic layer thickness was not constant a plot of R_q against electrode separation (see fig. 4B) shows that R_q does not scale with layer thickness. Interestingly there was a clear divide between the layer thickness of industrial samples and laboratory-made prototypes. It was decided to focus on the range of R_q values shown by industrial samples for commercial

relevance since the electric fields would be higher in the thinner layers associated with these MLCCs.
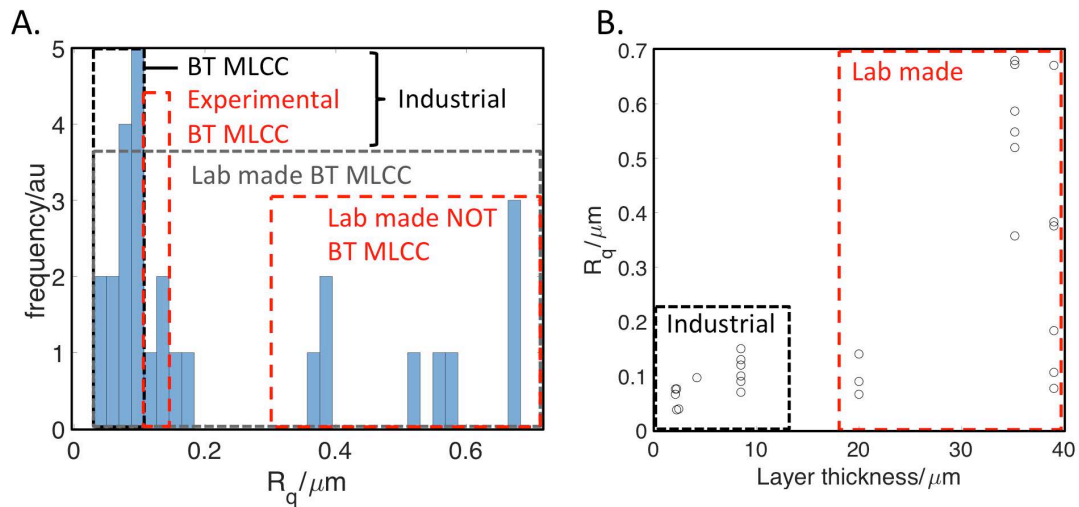
Fig. 4. (A) Histogram of the R_q values collected from the literature. (B) Plot of R_q versus layer thickness for the same micrographs.

3. Results:

Nyquist plots of impedance (see fig. 5A) and electric modulus (see fig. 5B) were simulated for interfaces with varying S_q values (see fig. 5C). A single incomplete arc associated with the response from the dielectric ceramics was observed in both plots. The arcs were incomplete, as the frequency range did not include values low enough to resolve the high resistivity of the ceramic. Whilst it is possible to go to frequencies lower than 0.05Hz using the FEM code, this is rarely practiced experimentally due to the length of time that lower frequency measurements take to perform. What can be deduced from these incomplete spectra is that the resistance of the dielectric layer (R_t, equal to the impedance arc diameter) decreases with increasing interface roughness whereas the capacitance of the dielectric layer (C_t, equal to the inverse of the electric modulus arc diameter) increases with increasing interface roughness. Fitting semicircles revealed the time constant for all models to be 1.30 s, in good agreement with the assigned material properties.
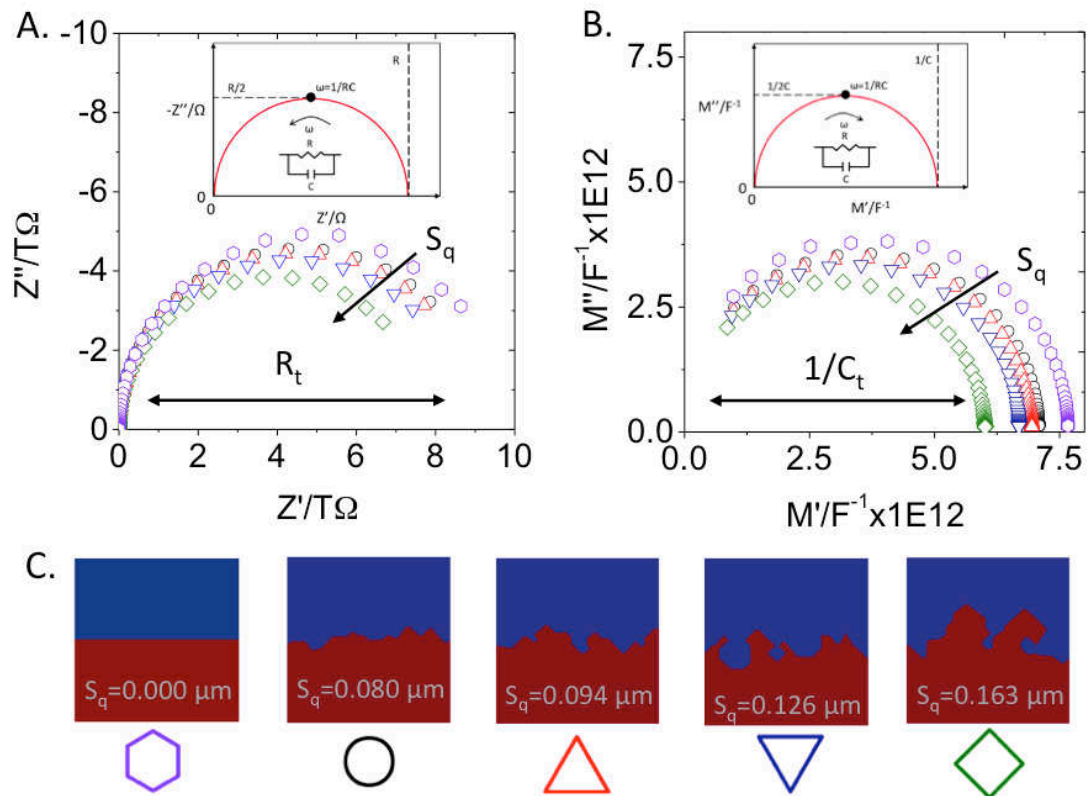
Fig. 5. Impedance (A) and electric modulus (B) Nyquist plots for interface roughness models with cross sections given in (C). The insets in (A) and (B) show the theoretical response for a single material that is electrically equivalent to a resistor and capacitor connected in parallel.

For a flat interface, DC simulations showed the electric field was homogenous in each layer with higher field strength in the ceramic (See fig. 6A). For a rough interface (see fig. 6B) the field was still higher in the ceramic layer but was heterogeneous. The point of maximum field was over twice the value for the flat ceramic layer and its position correlated with where the electrode had infiltrated the ceramic.
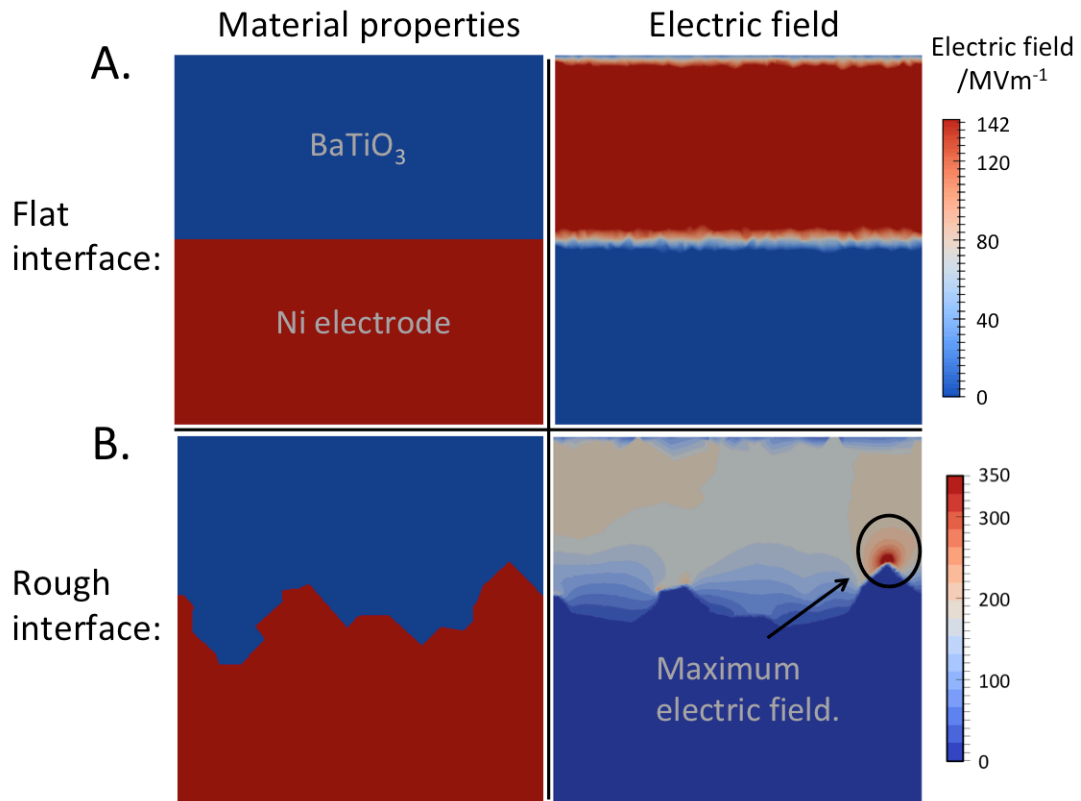
Fig. 6. Comparison of the physical microstructure and electric field distribution for (A) a flat interface and (B) a rough interface.

This analysis was repeated for all interfaces, finding the value of the maximum field magnitude, $\mathbf{E}_{max}$, which was then scaled by the same factor required to normalise the maximum field obtained in the flat layer model. $\mathbf{E}_{max}$ increased as the roughness increased (larger S_q) but there was significant scatter in the results (see fig. 7A). For each interface, the height of the point of maximum electric field in the Z axis direction of the model (Z_{max}, see fig. 2A) was identified and compared to the maximum interface amplitude. There was correlation between position of $\mathbf{E}_{max}$ and Z_{max} but $\mathbf{E}_{max}$ was not always located at the position of maximum amplitude (see fig. 7B).
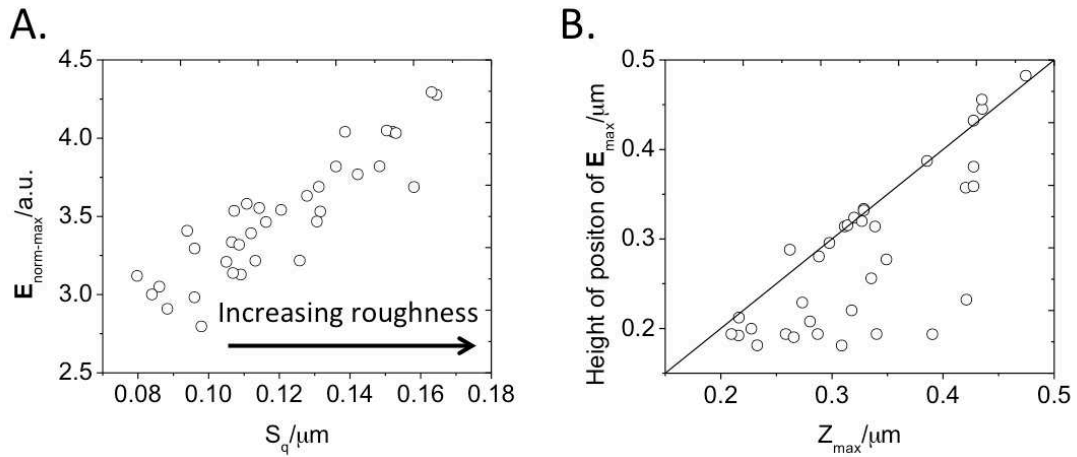
Fig. 7. (A) Maximum normalised electric field, E_{max}, versus interface roughness, S_q. (B) Height (with respect to the midplane defined in Fig 2) of the position of E_{max} versus the maximum interface amplitude for each model. The straight line indicates where the height of maximum field is the same as the maximum amplitude of a given interface, Z_{max}.

A benefit of the FEM approach is the ability to analyse the electrical microstructure (here the electric field) at any position or time step in the simulated physical microstructure. Here the electric field distribution in the ceramic layer has been studied quantitatively. We use the nodes of the FEM mesh that describes the ceramic to define positions within it. We measure the electric field strength at the position of each FEM node. We then scale all these points by the maximum field strength of the flat layer model as before. This gives us N_{mesh} values of the scaled electric field strength which we denote by $E_{norm}(i)$, where i=1,N_{mesh}. We then construct a probability histogram from these N_{mesh} values of E_{norm} which is shown in fig. 8.

In all histograms two peaks are observed, a peak at reduced field strength and a peak for enhanced values. As the roughness values increased (S_q increasing from 0.08 to 0.163 µm) the enhanced field peak reduced in height and became broader. It also shifted to values of higher field. For the roughest model (see fig. 8C) the electric field distribution was split into four regions (see fig. 9A). The first region included the small low field peak including up to 5% of the normalised field. The second region encompassed >5% to <100% of the normalised field strength. A third region consisted of the high field peak from 100% to 200% of the normalised field strength. Finally, the fourth region included the fields enhanced to over 200% of the normalised value. These regions were plotted (see fig. 9B) to show their locations within the physical microstructure.
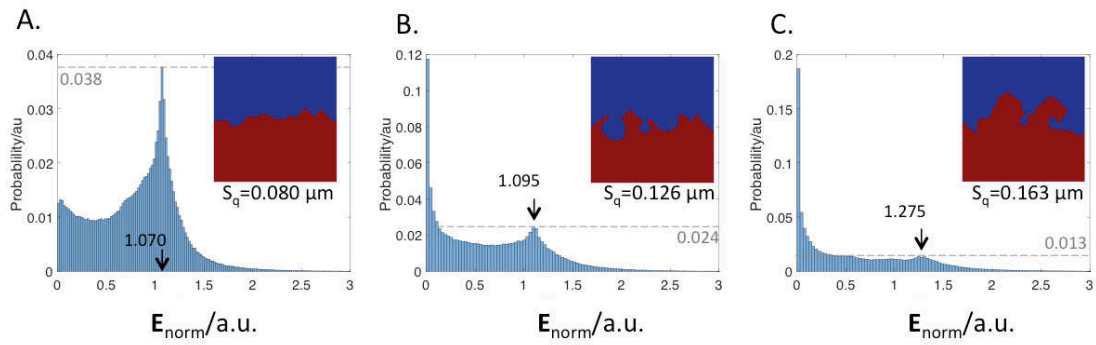
Fig. 8. Probability histograms for the electric field within the ceramic layer of several models with increasing interface roughness (A to C). The dashed line indicates the probability value of the rightmost peak discussed in the text and the arrow is the coinciding normalised field strength of the same peak. Note: the electric field has been normalised to the value within the ceramic layer for the flat interface model, E_{norm}.
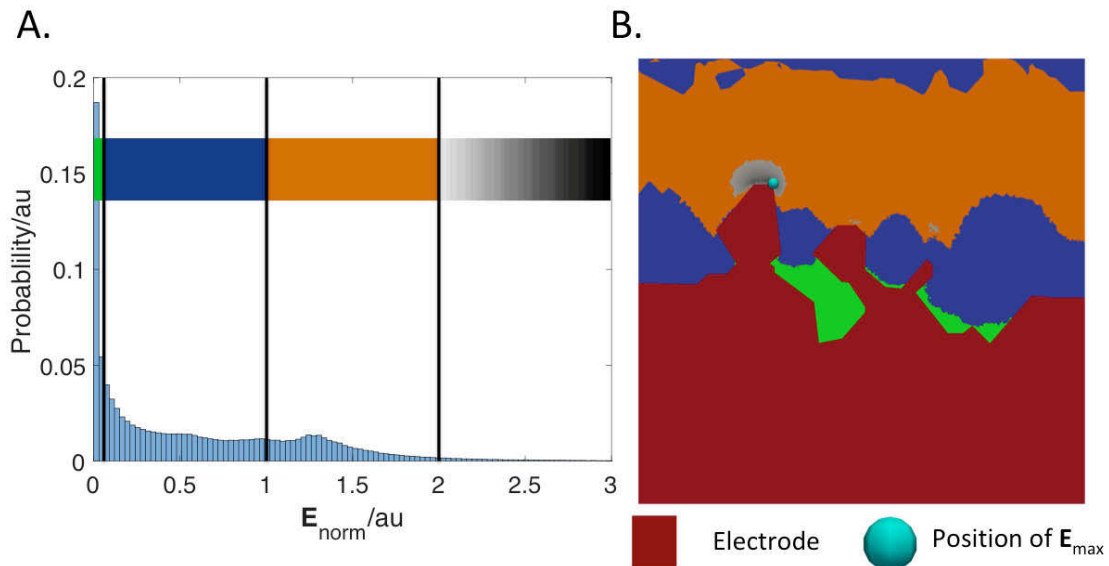
Fig. 9. (A) Probability histogram with different field strengths indicated with colours, note the grey scale for the larger field strengths. (B). Electric field plot of the ceramic layer where field values have been indicated using the legend in (A). The electrode (red) and the position of maximum field (cyan sphere) are shown for ease of visualisation.

4. Discussion:

2D profilometry analysis of interface roughness values of various MLCC micrographs shows that a range of R_q values is possible (see fig. 4A). Comparing the ceramic layer separation and R_q values showed a clear division between laboratory-made prototype and industrial capacitors. This is due to the miniaturisation required by industrial-scale fabrication and demonstrates highly optimised process control. Not all labs have access to tape casting equipment capable of one micron dielectric layer thickness. However, despite the disparity between the layer thickness of industrial and prototype capacitors, fig. 4B shows

there is a spread of R_q values for each group, implying the range of R_q values does not simply scale with layer thickness.

Impedance results (see fig. 5) are in good agreement with the sinusoidal interfaces studied by Samantaray[6], showing an increase in capacitance and reduction in resistance as the roughness increases. This can be explained simply by geometry. As the amplitude increases the electrode and ceramic become more interdigitated. As the roughness is continuous this results in a greater interface area and hence an enhanced electrode area giving rise to higher capacitance. An additional effect of the interdigitated interface is that, since the electrode is more conductive than the ceramic, easier conduction pathways form through the electrode material at the interface, bypassing the ceramic[5], resulting in up to a ~30% reduction of the dielectric layer's resistance in the interfacial region when compared to the flat layer model. This could be significant in multi-layer ceramic capacitors where individual ceramic layers between electrodes are commonly only a few microns thick.

Whilst the increase in capacitance is welcome for dielectric applications, the reduction in resistance can cause reliability issues. This is highlighted by the electric field strength enhancement of over fourfold (see figs. 6 and 7A). Generally electric field enhancement increased with amplitude roughness (quantified by S_q, see fig. 7A). However, plotting the Z coordinate of the position of maximum field against maximum amplitude (see fig. 7B) showed the position of maximum field was typically located close the interface for a given position (x,y) but it was not always at the highest amplitude in the interface for a given simulation. This is shown by the data points lying above and below the line $Z(E_{max}) = Z_{max}$ (i.e. the height of the position of maximum field equals the maximum interface amplitude), see fig. 7B.

The points that lie above or on this line are the easiest to explain. Here the part of the electrode that is highest, relative to the interface, offers an easier pathway for current to flow into the ceramic. This can be observed through a stream-trace of current density (see fig. 10A). Here the stream lines converge on the part of the electrode that offers an easy path, resulting in a large flux of current through itself (see bright regions in fig. 10B). Concentrated current flow will lead to high local electric fields in the ceramic layer above (see fig. 10C).
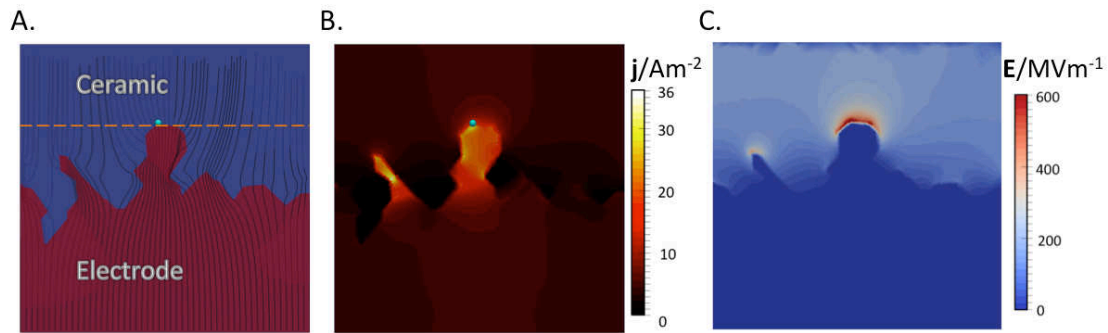
Fig. 10. (A) Interface where the point of maximum field (marked with a cyan sphere) occurs above the maximum interface amplitude (marked with a dashed line). Red denotes the electrode and blue denotes the ceramic. A stream trace of the current density is plotted in black lines. As the simulation is 3D the streamlines curve in and out of the plane of the plot, this is represented by a change in opacity. (B) DC current density plot of the same interface. (C) DC electric field distribution of the same interface. All plots are in the same vertical plane.

Local microstructural features cause the points of maximum field that are lower than the maximum interface amplitude. This is shown in fig. 11A where the position of maximum field correlates with a sharp electrode intrusion. While the current streamlines do converge into the base of this feature, the current density is focused as it flows into an increasingly smaller volume of electrode material (see fig. 11B). This results in an enhanced electric field in the ceramic just above the electrode "spike" (see thinner bright region fig. 11C).
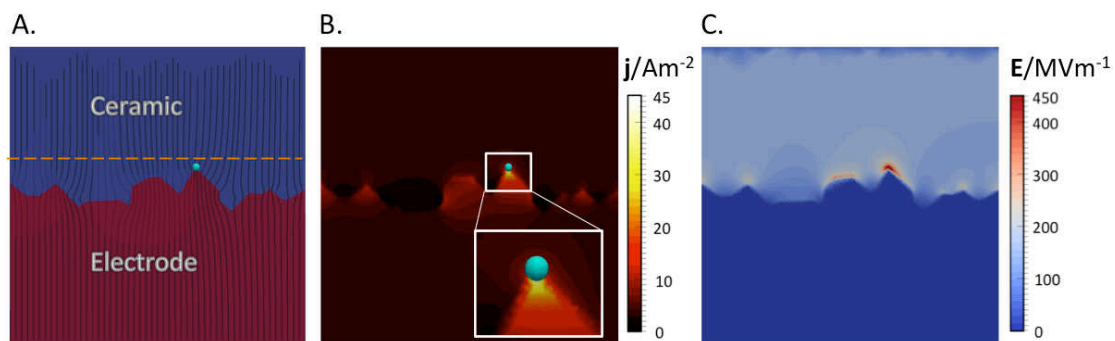
Fig. 11. (A) Interface where the point of maximum field (marked with cyan sphere) occurs below the maximum interface amplitude (marked with a dashed line). Red denotes the electrode and blue denotes the ceramic. A stream trace of the current density is plotted in black lines. As the simulation is 3D the streamlines curve in and out of the plane of the plot, this is represented by a change in opacity. Also, the position of maximum interface amplitude is not in this plane hence the dashed line is completely above the electrode. (B) DC current density plot of the same interface, inset is enlargement of area discussed in text. (C) DC electric field distribution of the same interface. All plots are in the same vertical plane.

The effect of local morphology can also be seen in the 3D microstructure of the electrode. Removal of the ceramic layer from the same interface is shown in fig. 11 reveals the electrode layer and the position of maximum field can be

seen and is indicated with a red sphere and a black arrow in fig. 12A and enhanced as a red circle and a black arrow in fig. 12B. Qualitative analysis shows there are features in the electrode that are higher than the point of maximum field but these are larger and more faceted regions (indicated with black circles). The position of maximum field is located at a much sharper (pointed) region.
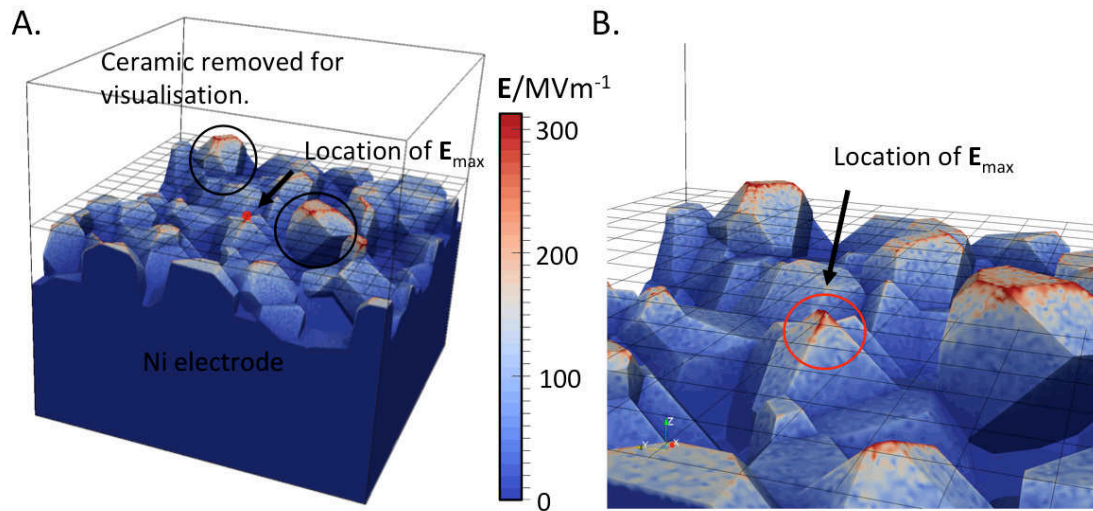
Fig. 12. (A) Location of maximum electric field for a given model marked with a red sphere. The grid height is the Z coordinate of the point of maximum field (Z_{max}). (B) Enlargement of (A) with red circle indicting the red sphere region shown in (A).

Analysis of the distribution of electric field shows the effect of roughness. As the amplitude roughness increases, the peak in the distribution relating to the enhanced electric field becomes shorter, broader and shifts to higher scaled field values (see figs. 8A-C). Thus, for rougher interfaces a greater proportion of the ceramic experiences greater field strength, making breakdown more likely to occur. It is also interesting to note the physical location of the different peaks (see fig. 9A). The peak corresponding to low field strength was located in the troughs of the electrode. The region of low field intensity between the two peaks was located in the ceramic adjacent to the electrode, not extending past any electrode intruding into the ceramic. The regions corresponding to the majority of the field values (that were enhanced up to 200% of the normalised field) were distributed in the ceramic above any intruding electrode. Finally, the remaining regions of electric field that had values greater than 200% of the normalised field were concentrated above the protruding parts of the electrode. Further work should be undertaken to determine whether the largest values of field (but with a low probability density) or those greater than the flat layer values (but make up the majority of high field values) are more important in break-down event(s).

5. Conclusions:

Finite element modelling has shown that an increase in amplitude roughness of the ceramic/electrode interface in MLCCs can cause an increase in electric field

strength of over four times. The largest enhancement of field occurs where parts of the electrode intrude into the ceramic layers. It is also noted there is a large region of enhanced field strength above any intrusions that has a higher field strength than a flat layer model. Stream traces of current density show the reason why the areas around the intrusions of an electrode are important. They provide an easy pathway for current to flow into, focusing the current into a small volume and increasing the local electric field. The local morphology is also an important factor as sharper (pointed) parts of the electrode also have higher local fields. Whilst it is impractical to suggest eliminating interface roughness in MLCCs entirely, it is advisable to minimise the roughness of the electrode layers and any intrusion of the electrode into the ceramic.

References:

References

1. H. Kishi, Y. Mizuno, and H. Chazono, "Base-metal electrode-multilayer ceramic capacitors: Past, present and future perspectives," *Japanese Journal of Applied Physics Part 1-Regular Papers Short Notes & Review Papers,* 42[1] 1-15 (2003).
2. C. A. Randall, S. F. Wang, D. Laubscher, J. P. Dougherty, and W. Huebner, "Structure Property Relationships in Core-Shell $BaTiO_3$-LiF Ceramics," *Journal of Materials Research,* 8[4] 871-79 (1993).
3. A. Golev, M. Scott, P. D. Erskine, S. H. Ali, and G. R. Ballantyne, "Rare earths supply chains: Current status, constraints and opportunities," *Resources Policy,* 41 52-59 (2014).
4. J. S. Dean, J. H. Harding, and D. C. Sinclair, "Simulation of Impedance Spectra for a Full Three- Dimensional Ceramic Microstructure Using a Finite Element Model," *Journal of the American Ceramic Society,* 97[3] 885-91 (2014).
5. J. P. Heath, J. S. Dean, J. H. Harding, and D. C. Sinclair, "Simulation of Impedance Spectra for Core-Shell Grain Structures Using FiniteElement Modeling," *Journal of the American Ceramic Society,* 98[6] 1925-31 (2015).
6. M. M. Samantaray, A. Gurav, E. C. Dickey, and C. A. Randall, "Electrode Defects in Multilayer Capacitors Part I: Modeling the Effect of Electrode Roughness and Porosity on Electric Field Enhancement and Leakage Current," *Journal of the American Ceramic Society,* 95[1] 257-63 (2012).
7. M. M. Samantaray, A. Gurav, E. C. Dickey, and C. A. Randall, "Electrode Defects in Multilayer Capacitors Part II: Finite Element Analysis of Local Field Enhancement and Leakage Current in Three-Dimensional Microstructures," *Journal of the American Ceramic Society,* 95[1] 264-68 (2012).

8. C. Geuzaine and J.-F. Remacle, "Gmsh: A 3-D finite element mesh generator with built-in pre- and post-processing facilities," *International Journal for Numerical Methods in Engineering,* 79[11] 1309-31 (2009).

9. G. Dale, M. Strawhorne, D. C. Sinclair, and J. S. Dean, "Finite element modeling on the effect of intra-granular porosity on the dielectric properties of $BaTiO_3$ MLCCs," *Journal of the American Ceramic Society,* 101[3] 1211-20 (2018).

10. C. S. Chiang, Y. C. Lee, F. T. Shiao, W. H. Lee, and D. Hennings, "Effect of TiO_2 doped Ni electrodes on the dielectric properties and microstructures of $(Ba_{0.96}Ca_{0.04})(Ti_{0.85}Zr_{0.15})O_3$ multilayer ceramic capacitors," *Journal of the European Ceramic Society,* 32[4] 865-73 (2012).

11. C. H. Rycroft, "VORO plus plus : A three-dimensional Voronoi cell library in C plus," *Chaos,* 19[4] (2009).

12. W. P. Dong, P. J. Sullivan, and K. J. Stout, "Comprehensive Study of Parameters for Characterizing 3-Dimensional Surface-Topography .3. Parameters for Characterizing Amplitude and Some Functional-Properties," *Wear,* 178[1-2] 29-43 (1994).

13. T. R. Albrecht, S. Akamine, T. E. Carver, and C. F. Quate, "Microfabrication of Cantilever Styli for the Atomic Force Microscope," *Journal of Vacuum Science & Technology a-Vacuum Surfaces and Films,* 8[4] 3386-96 (1990).

14. I. Stoica, E. G. Hitruc, D. Timpu, V. Barboiu, and D. S. Vasilescu, "Establishing proper scanning conditions in atomic force microscopy on polyimide and polyurethane samples and their effect on 3D surface texture parameters," *Scanning,* 37[5] 335-49 (2015).

15. K. Thornton and H. F. Poulsen, "Three-diemensional materials science: An intersection of three-dimensional reconstructions and simulations," *MRS Bulletin,* 33[6] 587-95 (2008).

16. Matlab, "version 9.3.0.713579 (R2017b).*"* The MathWorks Inc., (2017).

17. J. M. Prewitt, "Object enhancement and extraction," *Picture processing and Psychopictorics,* 10[1] 15-19 (1970).

18. S. H. Yoon, "Effect of Dy on the dielectric nonlinear behavior of Mn and V-doped $BaTiO_3$ multilayer ceramic capacitors," *Journal of Materials Research,* 30[16] 2447-55 (2015).

19. B. Y. Yu and W. C. J. Wei, "Defects of base metal electrode layers in multi-layer ceramic capacitor," *Journal of the American Ceramic Society,* 88[8] 2328-31 (2005).

20. C. C. Lin, W. C. J. Wei, C. Y. Su, and C. H. Hsueh, "Oxidation of Ni electrode in $BaTiO_3$ based multilayer ceramic capacitor (MLCC)," *Journal of Alloys and Compounds,* 485[1-2] 653-59 (2009).

21. Y. C. Lee, C. T. Lee, S. Wang, and F. S. Shieu, "A study of ceramic addition in end termination of multilayer ceramics capacitors with cofiring process," *Materials Chemistry and Physics,* 100[2-3] 355-60 (2006).

22. D. S. B. Heidary and C. A. Randall, "Redesigning Multilayer Ceramic Capacitors by Preservation of Electrode Conductivity and Localized Doping," *ACS Applied Materials & Interfaces,* 8[45] 31449-59 (2016).

23. W. P. Dong, P. J. Sullivan, and K. J. Stout, "Comprehensive Study of Parameters for Characterizing 3-dimensional Surface-topography .1. Some Inherent Properties of Parameter Variation," *Wear,* 159[2] 161-71 (1992).